J|A|C|S ARTICLES

Published on Web 02/18/2010

Structure-Based Calculations of Optical Spectra of Photosystem I Suggest an Asymmetric Light-Harvesting Process

Julian Adolphs,[†] Frank Müh,[†] Mohamed El-Amine Madjet,[†] Marcel Schmidt am Busch,[‡] and Thomas Renger*[,‡]

Institut für Chemie und Biochemie, Freie Universität Berlin, Fabeckstrasse 36a, D-14195 Berlin, Germany, and Institut für Theoretische Physik, Johannes Kepler Universität Linz, Altenberger Strasse 69, 4040 Linz, Austria

Received August 26, 2009; E-mail: thomas.renger@jku.at

Abstract: Optical line shape theory is combined with a quantum-chemical/electrostatic calculation of the site energies of the 96 chlorophyll *a* pigments and their excitonic couplings to simulate optical spectra of photosystem I core complexes from *Thermosynechococcus elongatus*. The absorbance, linear dichroism and circular dichroism spectra, calculated on the basis of the 2.5 Å crystal structure, match the experimental data semiquantitatively allowing for a detailed analysis of the pigment−protein interaction. The majority of site energies are determined by multiple interactions with a large number (>20) of amino acid residues, a result which demonstrates the importance of long-range electrostatic interactions. The low-energy exciton states of the antenna are found to be located at a nearest distance of about 25 Å from the special pair of the reaction center. The intermediate pigments form a high-energy bridge, the site energies of which are stabilized by a particularly large number (>100) of amino acid residues. The concentration of low energy exciton states in the antenna is larger on the side of the A-branch of the reaction center, implying an asymmetric delivery of excitation energy to the latter. This asymmetry in light-harvesting may provide the key for understanding the asymmetric use of the two branches in primary electron transfer reactions. Experiments are suggested to check for this possibility.

Introduction

In photosynthetic antennas, light is absorbed by pigments and the excitation energy is transferred to the photosynthetic reaction center (RC), where the conversion into chemical energy takes place. The crystal structure of the photosystem I (PSI) core complex from the thermophilic cyanobacterium *Thermosynechococcus (T.) elongatus*[1] revealed that this pigment−protein complex (PPC) binds both RC pigments and light harvesting antenna pigments inseparably on the same protein. This complex offers the possibility to study the interplay of light absorption, excitation energy transfer and trapping by electron transfer (ET) within one functional unit. However, the size and complexity of PSI is a challenge for theory.

The PSI core complex of *T. elongatus* is a trimeric complex, where each monomer consists of 12 protein subunits, that altogether bind 96 chlorophyll *a* (Chl*a*), 22 carotenoids, two phylloquinones, three iron−sulfur clusters and four lipids besides a number of water molecules. The two largest subunits, termed PsaA and PsaB, bind most of the core antenna pigments and redox-active cofactors of the RC.[1,2] The latter comprise the two special pair Chls P_A and P_B, the two accessory Chls Acc_A and Acc_B, the two electron acceptor Chls A_{0A} and A_{0B} and two phylloquinones A_{1A} and A_{1B} that are arranged in two symmetric branches termed A and B. At present the identity of the primary electron donor in PSI is debated in the literature.[3,4] Mutagenesis studies of the axial ligand to the special pair Chl P_B, of an aromatic residue in the neighborhood of the special pair and of a hydrogen bond donor to P_A did not show a difference in the primary charge transfer kinetics,[3] compared to the wildtype, whereas those of hydrogen bond donors to the electron acceptors A_{0A} and A_{0B} did.[4] These results were taken as evidence that the first ET step does not involve the special pair, that is, the accessory chlorophyll should be the primary electron donor. This suggestion, however, is difficult to reconcile with the fact that the special pair is assumed to create the excitation energy sink in the RC[5] most likely due to electron exchange (short-range) effects[6] as in the RC of purple bacteria. Whereas in purple bacteria and in photosystem II (i.e., in type II RCs) ET proceeds only along one of the two symmetric branches of the RC, in the type I RC of PSI most likely both branches are ET

[†] Freie Universität Berlin.
[‡] Johannes Kepler Universität Linz.

(1) Jordan, P.; Fromme, P.; Witt, H. T.; Klukas, O.; Saenger, W.; Krauss, N. *Nature* **2001**, *411*, 909.
(2) Golbeck, J. H., Ed. *Photosystem I: The Light-Driven Plastocyanin: Ferredoxin Oxidoreductase*; Springer: Dordrecht, The Netherlands, 2006.
(3) Holzwarth, A. R.; Müller, M. G.; Niklas, J.; Lubitz, W. *Biophys. J.* **2006**, *90*, 552.
(4) Luthra, R.; Narasimhulu, K.; Jasaitis, A.; Redding, K.; Ozarowski, A.; von Tol, J.; Rappaport, F.; Müller, M.; Slavov, C.; Holzwarth, A. *Photosynth. Res.* **2007**, *91*, 148.
(5) Witt, H.; Schlodder, E.; Teutloff, C.; Niklas, J.; Bordignon, E.; Carbonera, D.; Kohler, S.; Labahn, A.; Lubitz, W. *Biochemistry* **2002**, *41*, 8557.
(6) Madjet, M. E.; Müh, F.; Renger, T. *J. Phys. Chem. B* **2009**, *113*, 12603.

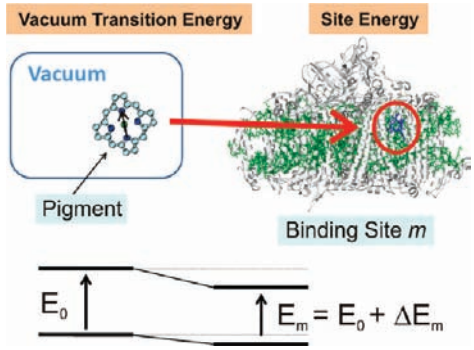

Figure 1. Vacuum transition energy E_0 of a pigment is changed by the local protein environment to its local transition energy (site energy E_m). In the CDC method, the shift of the transition energy ΔE_m is obtained as the difference in pigment−protein Coulomb couplings between the ground and excited states of the pigments. The pigments and the protein are represented by atomic partial charges that are obtained from fitting of *ab initio* electrostatic potentials.

active,[7−11] with a branching ratio that depends on the experimental conditions. There is general consensus about a more frequent occurrence of A-branch ET.[7−13] The reason for the asymmetric ET is unknown.

If one wants to model optical spectra of a PPC, one has to take into account the pigment−pigment (excitonic) as well as the pigment−protein (exciton-vibrational) coupling in an appropriate way. A challenge for line shape theory is the fact that both types of couplings are of similar magnitude. The coupling between optical transition densities of the pigments, leading to the formation of delocalized excited states, competes with the pigment−protein coupling that localizes the excited states. This localization is caused by static and dynamic disorder in local optical transition energies of the pigments and by shifts in the average transition energies of the pigments in different binding sites. The latter energies are therefore termed site energies (Figure 1). Whereas it is well-known how to treat localization effects due to site energy shifts and static disorder, the inclusion of a dynamic localization of excited states in exciton calculations of PPCs is still an open problem.

At present, the most appropriate way to treat dynamic localization effects in large PPCs is to introduce domains of strongly coupled pigments and to allow for exciton delocalization only between pigments in the same domain.[14,15] A pigment belongs to a certain domain if its excitonic coupling to at least one other pigment in the domain is larger than a certain threshold value V_c, which is assumed to be similar to the reorganization energy of the dynamic modulation of local transition energies. In this way, it is implicitly assumed that for weak excitonic coupling, the local coupling to the vibrations dephases any excitonic coherence.

The combination of pigment−pigment and pigment−protein coupling in the domains leads to lifetime broadening and vibrational sidebands in the homogeneous lineshapes of the domains that can be well described by a non-Markovian density matrix theory developed previously.[16] Besides the dynamic theory providing expressions for the line shape, the parameters entering the line shape functions are needed. Accurate methods have been developed for the calculation of the excitonic coupling between the pigments,[17,18] including the influence of the fast polarization of the protein and solvent. Site energies constitute another important parameter type in the calculation of optical spectra of PPCs. In the case of the FMO protein of green sulfur bacteria, containing seven excitonically coupled bacteriochlorophyll *a* (BChl*a*) pigments, it was possible after more than 30 years of research, to arrive at a common set of site energies in the literature based on a fit of optical spectra.[17,19−21] This set was recently confirmed by an independent direct structure-based calculation approach[18,22] that allowed to uncover the molecular basis of site energy shifts.

In the case of the 96 Chls of PSI, an extraction of site energies from a fit of optical spectra, of course, contains a large degree of ambiguity. Clearly, there will be more than one set of 96 site energies that describes the linear optical spectra, each containing only a few peaks. Therefore, the predictive power of site energies determined in such a way may be questionable. Nevertheless, the fitting approaches by Byrdin et al.[23] and Brüggemann et al.[24] provide a quantitative description of the experimental absorbance, linear dichroism (LD) and circular dichroism (CD) spectra. The structure-based methods applied so far[25,26] qualitatively fail to describe the experimental LD spectrum.

Byrdin et al.[23] performed a fit *by hand*, considering symmetry relations, axial ligands, H-bonding and functional arguments concerning the location of the so-called red Chls, that is, antenna Chls that give rise to an absorbance peak on the low-energy side of the main peak.[27−29] Brüggemann et al.[24] used a genetic algorithm after assigning some chromophores to the red-most states. Of course, a direct calculation of site energies from the

(7) Guergova-Kuras, M.; Boudreaux, B.; Joliot, A.; Joliot, P.; Redding, K. *Proc. Natl. Acad. Sci. U.S.A.* **2001**, *98*, 4437.
(8) Bautista, J. A.; Rappaport, F.; Guergova-Kuras, M.; Cohen, R. O.; Golbeck, J. H.; Wang, J. Y.; Beal, D.; Diner, B. A. *J. Biol. Chem.* **2005**, *280*, 20030.
(9) Li, Y.; van der Est, A.; Lucas, M. G.; Ramesh, V. M.; Gu, F.; Petrenko, A.; Lin, S.; Webber, A. N.; Rappaport, F.; Redding, K. *Proc. Natl. Acad. Sci. U.S.A.* **2006**, *103*, 2144.
(10) Rappaport, F.; Diner, B. A.; Redding, K. In *Photosystem I: The Light-Driven Plastocyanin: Ferredoxin Oxidoreductase*; Golbeck, J. H., Ed.; Springer: Dordrecht, The Netherlands, 2006; p. 223.
(11) Redding, K.; van der Est, A. In *Photosystem I: The Light-Driven Plastocyanin: Ferredoxin Oxidoreductase*; Golbeck, J. H., Ed.; Springer: Dordrecht, The Netherlands, 2006; p 413.
(12) Cohen, R. O.; Shen, G.; Golbeck, J. H.; Xu, W.; Chitnis, P. R.; Valieva, A. I.; van der Est, A.; Pushkar, Y.; Stehlik, D. *Biochemistry* **2004**, *43*, 4754.
(13) Dashdorj, N.; Xu, W.; Cohen, R. O.; Golbeck, J. H.; Savikhin, S. *Biophys. J.* **2005**, *88*, 1238.
(14) Yang, M.; Damjanovic, A.; Vaswani, H. M.; Fleming, G. R. *Biophys. J.* **2003**, *85*, 140.
(15) Raszewski, G.; Renger, T. *J. Am. Chem. Soc.* **2008**, *130*, 4431.
(16) Renger, T.; Marcus, R. A. *J. Chem. Phys.* **2002**, *116*, 9997.
(17) Adolphs, J.; Renger, T. *Biophys. J.* **2006**, *91*, 2778.
(18) Adolphs, J.; Müh, F.; Madjet, M. E.; Renger, T. *Photosynth. Res.* **2008**, *95*, 197.
(19) Louwe, R. J. W.; Vrieze, J.; Hoff, A. J.; Aartsma, T. J. *J. Phys. Chem. B* **1997**, *101*, 11280.
(20) Vulto, S. I. E.; de Baat, M. A.; Louwe, R. J. W.; Permentier, H. P.; Neef, T.; Miller, M.; van Amerongen, H.; Aartsma, T. J. *J. Phys. Chem. B* **1998**, *102*, 9577.
(21) Wendling, M.; Przyjalgowski, M. A.; Gülen, D.; Vulto, S. I. E.; Aartsma, T. J.; van Grondelle, R.; van Amerongen, H. *Photosynth. Res.* **2002**, *71*, 99.
(22) Müh, F.; Madjet, M. E.; Adolphs, J.; Abdurahman, A.; Rabenstein, B.; Ishikita, H.; Knapp, E. W.; Renger, T. *Proc. Natl. Acad. Sci. U.S.A.* **2007**, *104*, 16862.
(23) Byrdin, M.; Jordan, P.; Krauss, N.; Fromme, P.; Stehlik, D.; Schlodder, E. *Biophys. J.* **2002**, *83*, 433.
(24) Brüggemann, B.; Sznee, K.; Novoderezhkin, V.; van Grondelle, R.; May, V. *J. Phys. Chem. B* **2004**, *108*, 13536.
(25) Damjanovic, A.; Vaswani, H. M.; Fromme, P.; Fleming, G. R. *J. Phys. Chem. B* **2002**, *106*, 10251.
(26) Yin, S.; Dahlbom, M. G.; Canfield, P. J.; Hush, N. S.; Kobayashi, R.; Reimers, J. R. *J. Phys. Chem. B* **2007**, *111*, 9923.

structural data would be highly desirable to understand the building principle of the PSI antenna. However, such a calculation is difficult[25,26] because of the complexity of the pigment−protein coupling. Damjanovic et al.[25] used a semiempirical INDO/S quantum chemical method. In their approach, a cutoff radius of 2.5 Å was used and every amino acid with an atom within this distance of any atom of a given Chl was included in the quantum chemical calculation of the site energy of this Chl. Such a procedure neglects long-range electrostatic couplings that might be important.[18,22] In an alternative quantum chemical study, Yin et al.[26] used a semiempirical INDO as well as a time-dependent density functional theory (TDDFT) approach with the Coulomb attenuated CAM-B3LYP exchange correlation (XC) functional to calculate the site energies of PSI. The calculations were performed on a geometry-optimized structure of PSI and included the whole environment (protein, lipids, cofactors, water) of the Chls as partial charges. In this case, of course, long-range electrostatic effects were considered. However, the inclusion of classical point charges in quantum chemical calculations is not without problems, since the electron density of the Chls can be artificially distorted by these charges, an effect known as the electron leakage or spill out problem.[30] The above two methods provided a qualitatively correct description of the experimental absorbance spectrum, but both cannot describe the LD spectrum. Strong deviations are obtained, in particular, at short wavelengths (high energies).

Müh et al.[22] combined quantum chemical calculations on the pigments in vacuum with electrostatic Poisson−Boltzmann type calculations on the whole PPC in atomic detail, taking into account nonstandard protonation patterns of the titratable amino acid residues. The method was applied to the FMO protein. The resulting site energies of the seven BChl*a* pigments describe the experimental linear absorbance, linear dichroism and circular dichroism spectra quantitatively. The method by Müh et al.[22] was recently simplified in the so-called charge density coupling (CDC) method by Adolphs et al.[18] The CDC method yielded similar site energy values and reproduced the dominating influence of the electric field of the backbone of two α -helices. The latter was found[18,22] to determine the energy sink at BChl*a* 3 in the FMO protein. Based on the location of this energy sink, it was concluded that BChl*a* 3 is likely to be the linker pigment between the FMO protein and the core complex.[17] Recently, direct evidence for the proposed orientation of the FMO protein in the photosystem was obtained by chemical labeling and mass spectrometry.[31] In the present work, the CDC method, which was successfully tested on the seven BChl*a* of the FMO protein, is applied to obtain the site energies of the 96 Chl*a* of cyanobacterial PSI.

This work is organized in the following way. A brief summary of the theory of optical spectra is given first. Afterward, we describe the methods used to obtain the excitonic couplings and the site energies. These quantities are then applied in the calculation of optical spectra of PSI core complexes. Finally, we analyze the structural basis of site energy shifts in the PSI core complex and conclude the article.

Theory and Computational Methods

Linear Optical Spectra. In the following, a short survey of the theory used for the calculation of optical spectra is given. For a more detailed discussion, we refer to refs 15−17. The theory is based on a standard Hamiltonian for PPCs that models the pigments as coupled two-level systems interacting with vibrational degrees of freedom of the protein.

So far, there exists no theory of optical spectra that includes exciton-relaxation induced lifetime broadening and vibrational sidebands[32] as well as dynamic localization of exciton states[33] at the same time. As mentioned above, in the present work dynamic localization effects are treated implicitly by allowing delocalized states only to be formed between pigments m and n with an excitonic coupling $V_{mn} \geq V_c$. The threshold value V_c is chosen to be the reorganization energy $E_\lambda = \hbar \int d\omega J(\omega)\omega$ for a local transition derived from the spectral density $J(\omega)$ of the pigment−protein coupling. E_λ characterizes the strength of the modulation of the local transition energies of the pigments by the protein vibrations.

Once the *domains* of strongly coupled pigments are defined,[14,15] an optical spectrum of the whole complex is calculated as sum over the spectra of the single domains. The delocalized exciton states in domain d

$$|M_d\rangle = \sum_{m_d} c_{m_d}^{(M_d)} |m_d\rangle \tag{1}$$

are given as linear combinations of localized excited states $|m_d\rangle$. The absolute square of the coefficient $c_{m_d}^{(M_d)}$ gives the probability for the m_dth pigment to be excited when the domain is in the M_dth exciton state. The exciton coefficients and exciton energies are obtained by diagonalizing a matrix that contains the excitonic couplings $V_{m_d n_d}$ in the off-diagonal and the site energies E_{m_d} in the diagonal.[15,16]

The linear absorbance spectrum $\alpha(\omega)$ is obtained as:[15,16]

$$\alpha(\omega) \propto \omega \sum_d \langle \sum_{M_d} |\vec{\mu}_{M_d}|^2 D_{M_d}(\omega) \rangle_{\mathrm{dis}} \tag{2}$$

where the transition dipole moments of the delocalized exciton states $\vec{\mu}_{M_d} = \sum_{m_d} c_{m_d}^{(M_d)} \vec{\mu}_{m_d}$ are linear combinations of the local transition dipole moments $\vec{\mu}_{m_d}$. The latter are assumed to be oriented along the $N_B - N_D$ axis of the Chls,[34] and the sum over d denotes the summation over the spectra of the different domains.

The line shape function $D_{M_d}(\omega)$ includes lifetime broadening and vibrational sidebands as discussed in detail in refs 15 and 16. High-frequency intrachromophore vibrations are not taken into account, since they make only a small contribution to the low-energy region of the optical spectra studied here. Any conformational dynamics that is slow compared to the excited state lifetimes is included in $\langle ... \rangle_{\mathrm{dis}}$, which denotes an average over static disorder in site energies. A Gaussian distribution function is assumed for the latter and the average is performed by a Monte Carlo method.

The circular dichroism spectrum $CD(\omega)$ is obtained as

$$CD(\omega) \propto \omega \sum_d \langle \sum_{M_d} r_{M_d} D_{M_d}(\omega) \rangle_{\mathrm{dis}} \tag{3}$$

with the rotational strength $r_{M_d} = \sum_{m_d > n_d} c_{m_d}^{(M_d)} c_{n_d}^{(M_d)} \vec{R}_{m_d n_d} \cdot (\vec{\mu}_{m_d} \times \vec{\mu}_{n_d})$, where $\vec{R}_{m_d n_d}$ is the center-to-center distance vector connecting pigments m_d and n_d.

The linear dichroism spectrum $LD(\omega)$ reads

(27) Karapetyan, N. V.; Schlodder, E.; van Grondelle, R.; Dekker, J. P. In *Photosystem I: The Light-Driven Plastocyanin: Ferredoxin Oxidoreductase*; Golbeck, J. H., Ed.; Springer: Dordrecht, The Netherlands, 2006; p 177.
(28) Schlodder, E.; Shubin, V. V.; El-Mohsnawy, E.; Roegner, M.; Karapetyan, N. V. *Biochim. Biophys. Acta* **2007**, *1767*, 732.
(29) Brecht, M.; Studier, H.; Elli, A. F.; Jelezko, F.; Bittl, R. *Biochemistry* **2007**, *46*, 799.
(30) Neugebauer, J. *Chem. Phys. Chem.* **2009**, *10*, 3148.
(31) Wen, J.; Zhang, H.; Gross, M. L.; Blankenship, R. E. *Proc. Natl. Acad. Sci. U.S.A.* **2009**, *106*, 6134.
(32) Renger, T.; Marcus, R. A. *J. Phys. Chem. B* **2002**, *106*, 1809.
(33) Renger, T. *Phys. Rev. Lett.* **2004**, *93*, 188101.
(34) Madjet, M. E.; Abdurahman, A.; Renger, T. *J. Phys. Chem. B* **2006**, *110*, 17268.

$$LD(\omega) \propto \omega \sum_d \langle \sum_{M_d} |\vec{\mu}_{M_d}|^2 (1 - 3\cos^2 \theta_{M_d}) D_{M_d}(\omega) \rangle_{\mathrm{dis}} \quad (4)$$

where θ_{M_d} is the angle between the symmetry axis of the PSI-trimer (membrane normal) and the excitonic transition dipole moment $\vec{\mu}_{M_d}$.

Excitonic Couplings. Poisson-TrEsp Method. The excitonic couplings are obtained from the Coulomb couplings between the transition densities of the pigments. To take into account the influence of the dielectric, we introduced the following method:[17,18] The dielectric protein and solvent surrounding of the Chls is described by the same optical dielectric constant $\varepsilon_{\mathrm{opt}} = n^2 = 2$. We note that this value is in the interval [1.82, 2.04] estimated for $\varepsilon_{\mathrm{opt}}$ of PSI from an analysis[35] of the integral oscillator strength of protein-bound and solvent-extracted Chl*a*.[36] The Chls are modeled as vacuum cavities in the homogeneous dielectric containing the transition density (Figure 2). The transition density of Chl *m* is described by atomic transition charges $q_I(1, 0)$ that are located in the respective pigment cavities in the PSI complex, $\rho_m(\vec{r}) = \sum_I q_I(1, 0)\delta(\vec{r} - \vec{R}_I^{(m)})$, where $\vec{R}_I^{(m)}$ is the coordinate of the *I*th atom of pigment *m*. The transition charges $q_I(1, 0)$ are obtained by a three-dimensional fit of the electrostatic potential of the transition density obtained with time-dependent density functional theory and the B3LYP exchange correlation functional for fully geometry-optimized methyl-Chl*a*.[34] The transition charges are rescaled such as to result in the correct magnitude of the vacuum transition dipole strength of 21 D^2 as determined in an empty cavity analysis by Knox and Spring[37] from absorption data of Chl*a* in different solvents. Please note that such a rescaling relies on the fact that different quantum chemical methods were found to give very similar shapes but different magnitudes of the transition density.[34] The Poisson equation

$$\nabla \cdot [\varepsilon_{\mathrm{opt}}(\vec{r}) \nabla \phi_m(\vec{r})] = -4\pi \sum_I q_I \delta(\vec{r} - \vec{R}_I^{(m)}) \quad (5)$$

is solved for each Chl numerically by a finite difference method using the program MEAD.[38] The value of $\varepsilon_{\mathrm{opt}}(\vec{r})$ equals 2, if $\vec{r}$ points to a position in the protein or solvent, and 1, if $\vec{r}$ points into a Chl cavity. From the resulting electrostatic potential $\phi_m(\vec{r})$ of the transition density of Chl *m*, the excitonic coupling with Chl *n* is obtained as[17,18]

$$V_{mn} = \int d\vec{r}\, \phi_m(\vec{r}) \rho_n(\vec{r}) = \sum_I \phi_m(\vec{R}_I^{(n)}) q_I(1, 0) \quad (6)$$

The quantum chemical calculations were performed with the programs Jaguar[39] and QChem[40] and the fit of the electrostatic potential with CHELP-BOW.[41]

The results obtained by the above method, which we term Poisson-TrEsp, are compared with the results from point-dipole (PD) and extended-dipole (ED) approximations and with the couplings obtained with the TrEsp-method, described in the following.

Point-Dipole Approximation. In the simplest approach, the PD approximation, which is valid, if the distance between pigments is large compared to the extension of their transition densities, the excitonic coupling is given as

$$V_{mn} = f \frac{\mu_{\mathrm{vac}}^2}{R_{mn}^3} [\vec{e}_m \cdot \vec{e}_n - 3(\vec{e}_m \cdot \vec{e}_{mn})(\vec{e}_n \cdot \vec{e}_{mn})] \quad (7)$$

where $\vec{e}_m$ is a unit vector along the transition dipole moment of the *m*th Chl, the unit vector $\vec{e}_{mn}$ is oriented along the line connecting the centers of Chls *m* and *n*, μ_{vac}^2 is the dipole strength of the Q_y transition of Chl*a* in vacuum, and the factor *f* takes into account local field and screening effects in an effective way. In the simplest approximation, $f = 1/\varepsilon_{\mathrm{opt}}$, only screening effects are included. Accounting for local field corrections as well by using an empty spherical cavity model results in $f = 9\varepsilon_{\mathrm{opt}}/(2\varepsilon_{\mathrm{opt}} + 1)^2$,[42] that is, a factor $f = 0.72$ results for $\varepsilon_{\mathrm{opt}} = 2$.

Extended-Dipole Approximation. A first improvement of the PD approximation is the ED approximation. This approximation considers a certain extent of the pigment's transition density by placing two partial charges of opposite sign $\pm q$ at a distance *l* from each other and *l*/2 from the center of the molecule on the axis of the transition dipole moment ($N_B - N_D$). The magnitude of the charges $\pm q$ has to be chosen such as to yield the correct vacuum transition dipole moment magnitude $\mu_{\mathrm{vac}}^2 = (ql)^2 = 21\ D^2$ [37] of the $S_0 \rightarrow S_1$ transition of Chl*a*. A dipole extent of 8.7 Å was inferred for Chl*a* by Madjet et al.[34] The excitonic coupling is given by the Coulomb interaction between the partial charges of pigments *m* and *n*:

$$V_{mn} = f \sum_{i,j=1,2} (2\delta_{ij} - 1) \frac{q^2}{|r_m^{(i)} - r_n^{(j)}|} \quad (8)$$

where δ_{ij} is the Kronecker delta and $|r_m^{(i)} - r_n^{(j)}|$ is the distance between the partial charges $\pm q$ of pigments *m* and *n*.

TrEsp Method. In the transition-charges-from-electrostatic-potential (TrEsp) method, the Poisson equation (eq 5) is solved analytically for $\varepsilon_{\mathrm{opt}} = 1$ yielding $\phi_m(\vec{r}) = \sum_I q_I(1, 0)/|\vec{R}_I^{(m)} - \vec{r}|$ and the coupling is obtained from eq 6 as[34]

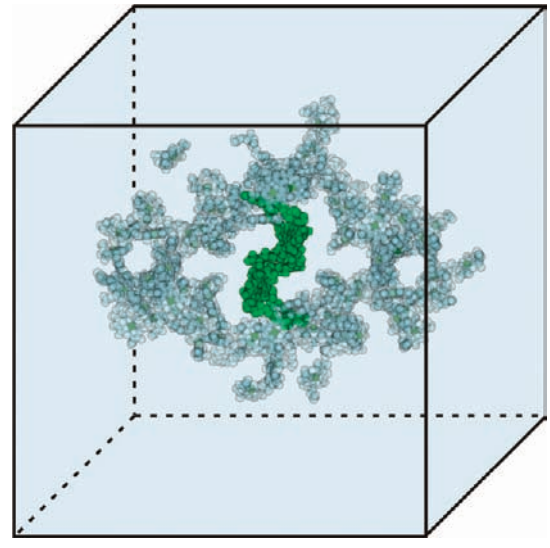

Figure 2. Dielectric volume considered in the calculations of excitonic couplings. The Chls are surrounded by protein and solvent, both described by an optical dielectric constant $\varepsilon_{\mathrm{opt}} = 2$. The chlorophyll-shaped cavities have $\varepsilon_{\mathrm{opt}} = 1$ inside and contain atomic transition charges derived from a fit of the electrostatic potential of the transition density, obtained with TDDFT using the B3LYP XC-functional. The transition charges are rescaled to yield the vacuum transition dipole moment inferred from experimental data. The cavities formed by the reaction center pigments are shown in green and those of the antenna pigments in blue-gray.

(35) Renger, T.; Madjet, M. E.; Müh, F.; Trostmann, I.; Schmitt, F. J.; Theiss, C.; Paulsen, H.; Eichler, H. J.; Knorr, A.; Renger, G. *J. Phys. Chem. B* **2009**, *113*, 9948.
(36) Müh, F.; Zouni, A. *Biochim. Biophys. Acta* **2005**, *1708*, 219.
(37) Knox, R. S.; Spring, B. Q. *Photochem. Photobiol.* **2003**, *77*, 497.
(38) Bashford, D. *Front. Biosci.* **2004**, *9*, 1082.
(39) *Jaguar 5.5*; Schrödinger, L.L.C.: Portland, OR, 1991−2003.
(40) Kong, J.; et al. *J. Comput. Chem.* **2000**, *21*, 1532.
(41) Sigfridsson, E.; Ryde, U. *J. Comput. Chem.* **1998**, *19*, 377.

$$V_{mn} = f\sum_{I,J}\frac{q_I(1,0)q_J(1,0)}{|R_I^{(m)} - R_J^{(n)}|} \quad (9)$$

where, in addition, a factor f was introduced to take into account the electronic polarizability of the environment in an implicit way as discussed above.

We note that, in general, the screening/local field correction factor f appearing in eqs 7, 8 and 9 is distance and orientation dependent.[43] However, our previous calculations on the FMO protein showed that the important nearest neighbor couplings may be approximated by the same f. This finding is supported by the present work on the basis of a comparison of TrEsp (eq 9) and Poisson-TrEsp (eq 5 and 6) calculations, as will be shown below.

Structure-Based Calculation of Site Energies: Charge Density Coupling. In the following, the structure-based method described in detail previously[18] is summarized. It aims at a direct calculation of site energies from the structural data. In this approach, no absolute site energies, but site energy shifts are calculated. The site energy E_m for Chl m is given by:

$$E_m = E_0 + \Delta E_m \quad (10)$$

where the site energy shift ΔE_m is obtained by the method described below, and the constant E_0, reflecting the transition energy in vacuum, is assumed to be equal for all Chls and will be inferred by comparing the center of the calculated and experimental spectra.

In the CDC method, quantum chemistry on Chl*a* in vacuum is combined with electrostatic calculations on the whole PPC in atomic detail. Polarization effects of the solvent and the protein are included in the calculation of the CDC by an effective dielectric constant ε_{eff}. In the original version of the CDC method,[18] a standard protonation pattern is assumed for the titratable amino acid residues of the protein. This standard state is defined as the protonation state that a residue would have in water at pH 7. In this case, Asp and Glu are deprotonated and negatively charged, Arg and Lys are protonated and positively charged, and for His we assumed that it is singly protonated and neutral. In the present work, we also consider nonstandard protonation patterns (see below).

To evaluate the CDC leading to the site energy shift ΔE_m, two sets of partial charges are needed, $\{\Delta q_l^{(m)}\}$ and $\{q_J^{(\text{bg})}\}$. The $\Delta q_l^{(m)} = q_l^{(m)}(1,1) - q_l^{(m)}(0,0)$ describe the change in charge density of the PPC when Chl m is excited. It is nonzero only on the macrocycle of Chl m. In the present work, these charges are assumed to be independent of the site, that is, $\Delta q_l^{(m)} = \Delta q_l$ for all m. The remaining charge density of the PPC is described by the background charges $q_J^{(\text{bg})}$ that include the whole protein, carotenoids, lipids, water molecules and all Chls $n \neq m$ in the ground state as well as the phytyl chain of Chl m.

The electrochromic shift of the mth pigment is calculated from the Coulomb interaction of the difference of ground and excited state charge density of pigment m, described by partial charges Δq_l, with the background charge density, described by the partial charges $q_J^{(\text{bg})}$

$$\Delta E_m = \frac{1}{\varepsilon_{\text{eff}}}\sum_{J=1}^{K}\Delta\phi_m(R_J^{(bg)})q_J^{(bg)} \quad (11)$$

where the difference in electrostatic potential $\Delta\phi_m(r)$ between the excited and the ground state of Chl m is given as

$$\Delta\phi_m(r) = \sum_{I=1}^{N}\frac{\Delta q_I}{|R_I^{(m)} - r|} \quad (12)$$

Here, N is the number of partial charges of the macrocycle of Chl m, K is the number of background partial charges and $R_I^{(m)}$ and $R_J^{(\text{bg})}$ define the location of the Ith difference partial charge of the mth pigment and the Jth partial charge of the background, respectively.

Calculations are based on the 2.5 Å crystal structure of PSI from *T. elongatus*,[1] where corrected coordinates are used for the Chl*a*' epimer of pigment number 1 provided by N. Krauss. The corrected coordinates were published very recently.[6] Hydrogen atoms were added by using CHARMM.[44,45] The structural model contains, besides protein and cofactors, 35 explicit water molecules that were chosen, because they are either axial ligands or hydrogen bond donors to Chl*a*. Subunit PsaK could not be completely modeled at 2.5 Å[1] and, therefore, is taken into account as poly-Ala fragments.

The background charges of the protein and the water are taken from the CHARMM22 force field,[45] and those of cofactors except Chl*a* where taken from Ishikita and Knapp.[46] The atomic partial charges of the Chls (Supporting Information (SI) Table 1) are obtained from a fit of the *ab initio* electrostatic potential of the ground and excited state charge densities, as described in detail in ref 34. The quantum chemical calculations are performed on Chl*a* in vacuum with the phytyl chain replaced by a methyl group (methyl-Chl*a*). Ground state geometries are obtained using density functional theory with the B3LYP XC-functional. Excited states are calculated using TDDFT with B3LYP, BHHLYP and B65LYP XC-functionals or Hartree−Fock (HF) with configuration interaction of single excitations (CIS). A detailed description of the XC-functionals is given in ref 6. We note that the different quantum chemical methods yield different difference dipole moments $\Delta\mu$ between ground and excited states of Chl*a*. In principle, it would be possible to rescale the difference charges $\Delta q_l^{(m)}$ such that the resulting $\Delta\mu$ matches the experimental value $\Delta\mu \approx 1$ D.[47] In the present calculations, this rescaling is implicitly included in the free parameter ε_{eff} in eq 11. The value of ε_{eff} is chosen such that the width of the calculated spectra matches that of the experimental ones.

Since under physiological conditions the titratable residues are not necessarily in the standard protonation state (defined above), because of electrostatic interactions with their environment and with each other, we determined the most probable protonation states of PSI at pH 4.0, 6.5, and 9.0 for $T = 300$ K following the methods of ref 22 with $\varepsilon_{\text{protein}} = 4.0$ and $\varepsilon_{\text{solv}} = 80.0$. A dielectric constant of $\varepsilon_{\text{mem}} = 2.0$ was assigned to a volume outside the PSI protein to mimic the dielectric properties of the thylakoid membrane (or detergent phase), which is dominated by alkyl chains (hydrocarbon phase).

We note that the use of different dielectric constants in the different parts of the calculations is not an inconsistency, but physically justified. The optical dielectric constant ε_{opt} represents the fast electronic polarizability of the protein, which is the only part of the polarizability relevant for the excitonic couplings between optical transitions. In contrast, the evaluation of protonation states, which are assumed to be in thermal equilibrium, requires the use of the static dielectric constants $\varepsilon_{\text{protein}}$, $\varepsilon_{\text{solv}}$ and ε_{mem}, representing the total (electronic, atomic and orientational) polarization of the protein, solvent and membrane medium. In particular, the value of $\varepsilon_{\text{protein}} = 4.0$ is a standard value in this type of calculations (e.g., refs 48−50 and references therein) that can be justified by microscopic molecular mechanics models.[51−53] Another dielectric constant ε_{eff} of the protein is applied in the site energy calculations.

(42) Jackson, J. D. *Classical Electrodynamics*, second edition, John Wiley & Sons: New York, 1975; p 147.
(43) Scholes, G. D.; Curutchet, C.; Mennucci, B.; Cammi, R.; Tomasi, J. *J. Phys. Chem. B* **2007**, *111*, 6978.
(44) Brooks, B. R.; Bruccoleri, R. E.; Olafson, B. D.; States, D. J.; Swaminathan, S.; Karplus, M. *J. Comput. Chem.* **1983**, *4*, 187.
(45) MacKerell, A. D., Jr.; et al. *J. Phys. Chem. B* **1998**, *102*, 3586.
(46) Ishikita, H.; Knapp, E. W. *J. Biol. Chem.* **2003**, *278*, 52002.
(47) Krawczyk, S. *Biochim. Biophys. Acta* **1991**, *1056*, 64.

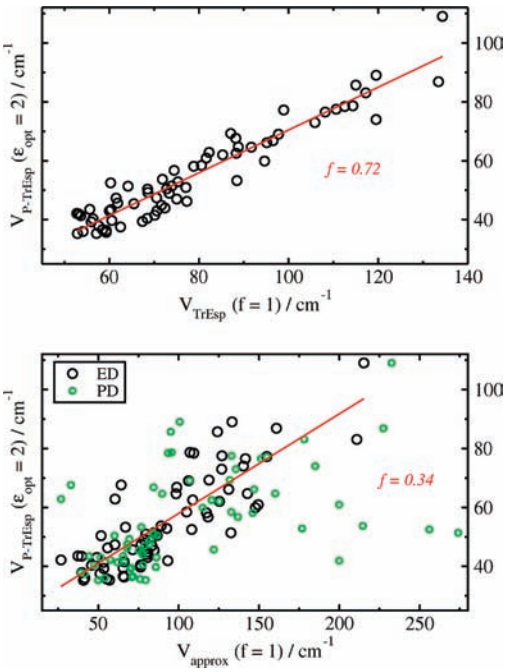

Figure 3. (Top) Correlation between excitonic couplings $V_{P-TrEsp}$ in a dielectric medium with $\varepsilon_{opt} = 2$ obtained with the Poisson-TrEsp method (eq 5 and 6) and vacuum couplings V_{TrEsp} obtained with the TrEsp method (eq 9, $f = 1$). (Bottom) Correlation of couplings $V_{P-TrEsp}$ with vacuum couplings V_{approx} in extended-dipole (ED, eq 8, $f = 1$) and point-dipole (PD, eq 7, $f = 1$) approximation. The red lines show linear regression fits that result in $f = 0.72$ for TrEsp and $f = 0.34$ for ED.

As discussed previously,[18] this ε_{eff} is essentially a fit parameter that effectively takes into account local field and screening effects, a correction of inaccuracies in the quantum chemical partial charges, and the nonequilibrium nature of the polarization in the protein for excited states of the pigments.

The calculations of protonation probabilities were performed with the programs TAPBS[48] and Karlsberg 2.[49] Further details of this type of calculation will be published elsewhere (F. Müh, M.E. Madjet, T. Renger, in preparation).

Results

Excitonic Couplings. The excitonic couplings are calculated either for vacuum ($\varepsilon_{opt} = 1$) or for a dielectric medium ($\varepsilon_{opt} = 2$) representing the protein and the solvent. The vacuum couplings are calculated with the TrEsp method (eq 9), the ED (eq 8) and the PD (eq 7) approximations using $f = 1$. These couplings are compared with the excitonic couplings obtained with the Poisson-TrEsp method in a dielectric with $\varepsilon_{opt} = 2$, in order to infer the factor f.

The results for these various calculations are presented in Figure 3 (SI Table 2). There is a strong correlation between the Poisson-TrEsp and the TrEsp couplings (Figure 3, upper panel), a weak correlation between the Poisson-TrEsp and the ED couplings and almost no correlation between the Poisson-TrEsp and the PD couplings (Figure 3, lower panel). To elucidate the factor f, a least mean square fit, $V_{mn}^{P-TrEsp}(\varepsilon_{opt} = 2) = fV_{mn}^{TrEsp}(\varepsilon_{opt} = 1)$ was performed with the couplings larger than the threshold value of $V_c = 35$ cm^{-1} (used in the definition of exciton domains, see below). This procedure results in a factor $f = 0.72$ (Figure 3, upper panel). If the couplings $V_{mn} < V_c$ are also included, the least mean square fit yields $f = 0.69$. Note that the small excitonic couplings have no influence on the calculated spectra, but may become important in the calculation of energy transfer rates.[15] The special pair coupling (i.e., that between Chl 1 and 2) was not included in the estimation of the f-factors, since it is dominated by short-range effects.[6]

The maximal difference between Poisson-TrEsp couplings and TrEsp couplings, using eq 9 with $f = 0.72$, is 12 cm^{-1} (coupling 38−53 and 44−45), that is, the couplings of PSI can be obtained in good approximation by the TrEsp method (see SI Figure S14 for a comparison of spectra) taking into account the polarizability of the environment implicitly by the above factor f. By comparing the Poisson-TrEsp couplings with the values obtained in PD and ED approximation (Figure 3, lower panel) it is seen that the PD approximation is invalid for PSI. Although in ED approximation the correlation with respect to the Poisson-TrEsp values is larger, it is still significantly lower than for the TrEsp couplings.

Site Energies and Optical Spectra of PSI. In the following, the CDC method is used to calculate the site energies of the 96 Chl*a* in PSI. These site energies are used together with the excitonic couplings to simulate optical spectra using the line shape theory described above. The site energies, which represent vertical transition energies of the pigments at the equilibrium position of nuclei in the electronic ground state, provide the diagonal part of the exciton Hamiltonian, whereas the excitonic couplings define the off-diagonal elements, as discussed above.

The same functional form of the spectral density $J(\omega)$ of the pigment−protein coupling, as determined previously[16] from a fit of fluorescence line narrowing spectra of the B777-complex, is used in the calculation of the line shape function $D_{M_d}(\omega)$. This spectral density has been applied successfully to a number of complexes like photosystem II,[15,54] the FMO protein[17,22] (for a comparison with fluorescence line narrowing spectra of the FMO protein, see ref 17) and the water-soluble chlorophyll binding protein.[35,55] We note that the inhomogeneous spectra calculated in the present work do not depend critically on the exact shape of the spectral density.

The integral of $J(\omega)$, that is, the Huang−Rhys factor $S = \int d\omega J(\omega)$, is estimated from the temperature dependence of the linear absorbance spectrum (SI Figure S15) to be $S = 0.6$. A reorganization energy $E_\lambda = 35$ cm^{-1} is obtained for this spectral density. Using $V_c = 35$ cm^{-1} results in 34 exciton domains where 17 domains contain at least 2 pigments (SI Table 2) and the remaining domains are single pigment domains. We note that the shape of the spectra does not critically depend on the exact value of V_c (SI Figure S16). The largest domain contains 13 pigments (SI Table 2). An equal inhomogeneous widths of 300 cm^{-1} (fwhm) for the distribution function of site energies is assumed for all pigments. This value was determined on the basis of a comparison of calculated and experimental spectra, i.e., it is a fit parameter in our calculations. The choice of this parameter influences the optimal value of ε_{eff}, which is also obtained from a fit of the experimental data. A smaller value of the inhomogeneous broadening results in a smaller value of ε_{eff}.

(48) Kieseritzky, G.; Knapp, E. W. *Proteins* **2008**, *71*, 1335.
(49) Rabenstein, B.; Knapp, E. W. *Biophys. J.* **2001**, *80*, 1141.
(50) Ullmann, G. M.; Knapp, E. W. *Eur. Biophys. J.* **1999**, *28*, 533.
(51) Simonson, T.; Brooks, C. L., III *J. Am. Chem. Soc.* **1996**, *118*, 8452.
(52) Simonson, T. *Rep. Prog. Phys.* **2003**, *66*, 737.
(53) Sham, Y. Y.; Chu, Z. T.; Warshel, A. *J. Phys. Chem. B.* **1997**, *101*, 4458.
(54) Renger, T.; Marcus, R. A. *J. Phys. Chem. B* **2002**, *106*, 1809.
(55) Renger, T.; Trostmann, I.; Theiss, C.; Madjet, M. E.; Richter, M.; Paulsen, H.; Eichler, H. J.; Knorr, A.; Renger, G. *J. Phys. Chem. B* **2007**, *111*, 10487.

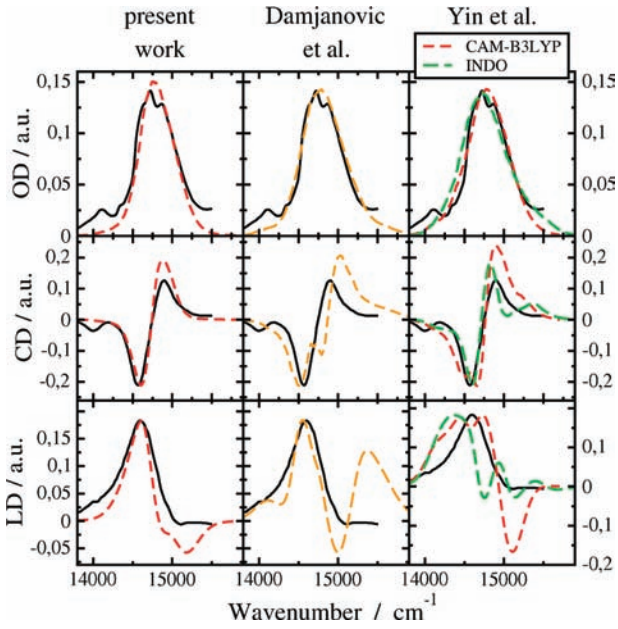

Figure 4. Absorbance (5 K), CD (77 K) and LD (295 K) spectra simulated (dashed lines) with different sets of site energies in comparison with experimental data[23] (black solid lines). (Left) Site energies from the CDC method using the TDDFT/B65LYP charges (SI Table 4). (Middle) Site energies from Damjanovic et al.[25] (Right) Site energies from Yin et al.[26] using TDDFT/CAM-B3LYP (red dashed lines) or semiempirical INDO (green dashed lines).

Values of the former down to 200 cm^{-1} give still reasonable agreement with experimental spectra (SI, Figure S17).

The spectra calculated using the above parameters and charges Δq_l derived from TDDFT/B65LYP are compared with experimental data[23] in the left part of Figure 4. There is a good semiquantitative agreement between theory and experiment. In particular, the main features of the experimental CD and LD spectra are well reproduced by the calculations. Deviations are observed at the red edge of each spectrum representing the *red* Chls.[27−29] Since the excited states of the latter are likely determined by short-range interactions[6] not included in the present electrostatic calculations, these deviations are expected. There are also some residual discrepancies between experiment and calculation in other regions of the spectra, especially at the blue edge of the LD spectrum. Calculations were also performed with charges Δq_l derived from TDDFT with other XC-functionals (B3LYP and BHHLYP) as well as with the wave function-based method HF-CIS. The spectra calculated with the different sets of site energies are very similar and deviate to a lesser extent from each other than from experiment (see SI Figure S18 for comparison of spectra and SI Figure S19 for correlation plots of site energies).

For a comparison of our approach to a structure-based calculation of site energies with those reported earlier in the literature, we computed spectra by using our excitonic couplings and line shape theory, but the different sets of site energies published by Damjanovic et al.[25] and Yin et al.[26] The results are shown in the middle and right panels of Figure 4. Whereas a qualitatively correct description of the experimental absorbance spectrum is achieved with all sets of site energies, only the present set (numerical values are given in SI Table 4) is capable of describing the CD and LD spectra well. The solely quantum chemical methods[25,26] fail particularly in the description of the LD spectrum. In ref 26, both site energies and excitonic couplings were calculated quantum chemically and a simpler line shape theory was used for the calculation of the spectra, resulting in an even poorer description of the LD spectrum (SI Figure S20). No CD and LD spectra were calculated in ref 25.

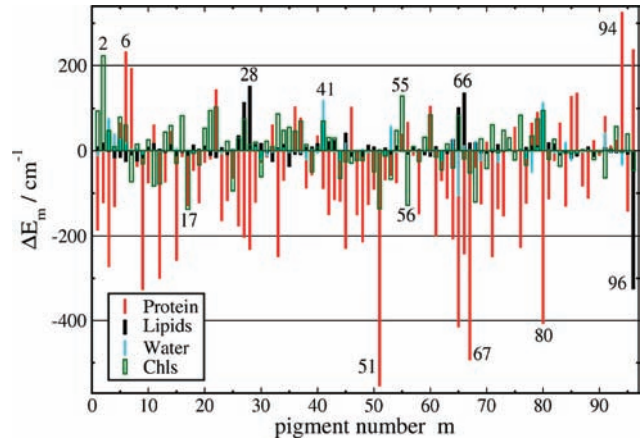

Figure 5. Site energy shifts ΔE_m^{Prot} caused by the protein, ΔE_m^{Chl} by Chls, ΔE_m^{Lip} by lipids and ΔE_m^{Wat} by explicit water molecules in units of cm^{-1} ($\varepsilon_{eff} = 1.5$). The numerical values are listed in SI Table 5.

Influence of Certain Parts of the PPC. The semiquantitatively correct description of the optical spectra, we think, makes a detailed analysis of the structure−function relationships on the basis of the calculated site energies reasonable. Here, we investigate the influence of the protein, the backbone of the α-helices, lipids, Chls and explicit water molecules. The analysis is performed for the site energies obtained with the TDDFT/B65LYP partial charges. Throughout this work, the pigments are numbered by $m = 1-96$, keeping the same order as in the structure file 1JB0.pdb (for a direct comparison with the pigment number in the structure file, see SI Table 4). In Figure 5, the site energy shifts ΔE_m caused by the protein, lipids, water and Chls are compared (numerical values are given in SI Table 5). In most cases the influence of the protein dominates the ΔE_m. The interaction with the protein leads to red-shifted site energies in the majority of sites ($\sum_m \Delta E_m^{Prot} \approx -7200\ cm^{-1}$), whereas Chls ($\sum_m \Delta E_m^{Chl} \approx +800\ cm^{-1}$), lipids ($\sum_m \Delta E_m^{Lip} \approx +300\ cm^{-1}$) and explicit water molecules ($\sum_m \Delta E_m^{Wat} \approx +200\ cm^{-1}$) preferentially lead to blue shifts.

For all 96 Chls, we determined the number N_{AARs} of amino acid contributions that at least must be accumulated (sorted with respect to their absolute value) to end up in an interval of $\pm 100\ cm^{-1}$ around the total site energy shift caused by all amino acid residues. For the large majority of pigments, the site energy shift has contributions from a large number of different residues, as shown in Figure 6. For 21 Chls the site energies are determined by 11−20 amino acid residues, 56 Chls have site energies which are caused by more than 20 amino acid residues, while 24 site energy shifts are caused by even more than 50 residues. For the reaction center pigments 3 (Acc_A), 4 (Acc_B), 5 (A_{0A}), and 6 (A_{0B}), as well as for both so-called *linker* or *bridging* Chls 46 (1140, A40) and 85 (1239, B39), the contribution of the protein to the site energy shift is further analyzed in Figure 7. In any of these cases, the contributions of more than 100 residues have to be summed up to approach the overall site energy shift caused by the protein. Hence the site energies of these pigments are stabilized by interactions with a particularly large number of amino acid residues.

The influence of α-helices on site energy shifts is not as dominant as in the FMO protein[18,22] (SI Figure S21). Nevertheless, the site energy of Chl 65, which is the third lowest site

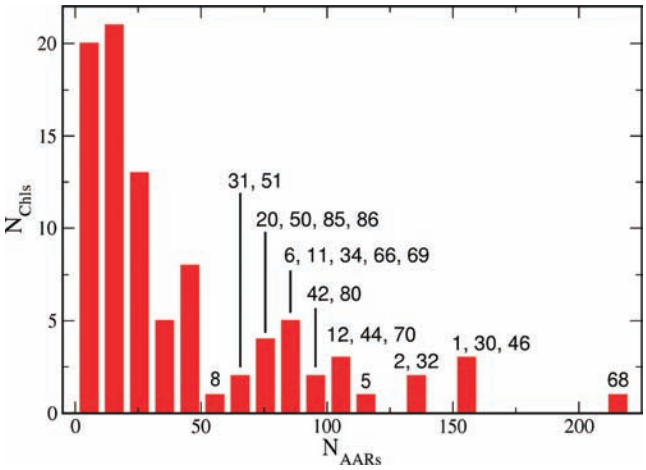

Figure 6. Number of Chls (N_{Chls}) for which N_{AARs} amino acid residues have large contributions to the site energy shift. The sum over these contributions is in an interval of ± 100 cm^{-1} of the total site energy shift. The black numbers are the numbers of the respective Chls.

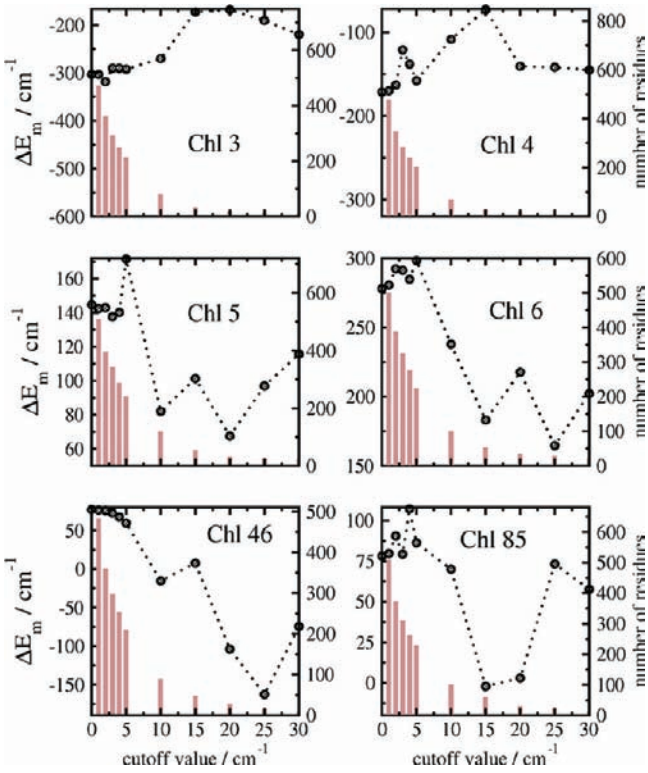

Figure 7. (Black circles) Sum over contributions of single amino acid residues to the site energy shifts of RC Chls 3−6 (Acc_A, Acc_B, A_{0A}, A_{0B}) and the bridging Chls 46, 85 (A40, B39), where only those single residue contributions are taken into account, that are larger than the cutoff value. The sum is shown as a function of the cutoff value in units of cm^{-1} (left *y*-axis). (Brown bars) Number of residues (right *y*-axis) that have a contribution larger than the cutoff value ($\varepsilon_{eff} = 1.5$).

energy of all pigments, contains a large contribution (−230 cm^{-1} out of the shift of −430 cm^{-1} of all amino acids) from the interaction with the backbones of α-helices, in particular with that of residues Gly B316−Met B320 (−200 cm^{-1}). The red-shift results from the positive end of the helix dipole, which is situated in the negative region of the difference potential $\Delta\phi_{65}$ of Chl 65 (Figure 8). The contributions of the backbones of the transmembrane helices to the site energy shifts are rather small because these helices are arranged in an antiparallel manner

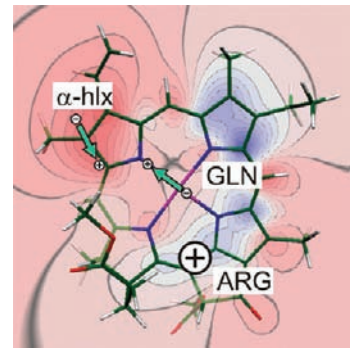

Figure 8. Difference in electrostatic potential $\Delta\phi(r)$ (eq 12) between excited state S_1 and ground state S_0 of Chl*a* (obtained with TDDFT using the B65LYP XC-functional) shown as a contour plot in the plane of the macrocycle. (Blue) Positive potential values. (Red) Negative potential values. For Chl 94, the main part of the large blue-shift of its site energy is caused by the positively charged Arg M24, which is placed in the positive difference potential. For Chl 12, the red-shift is mainly caused by the amide dipole of the side chain of Gln A115, while for Chl 65 the red-shift is mainly caused by the dipole of a short α-helix (Gly B316 - Met B320).

leading to partial cancellation effects (SI Figure S22). The remaining parts of the protein backbone also do not lead to large site energy shifts.

To investigate, whether single amino acid residues have a large influence on site energy shifts, we compared all contributions from single residues that are larger than 100 cm^{-1} with the total site energy shift of the respective pigment. We found 14 pigments for which the total shift is larger than 100 cm^{-1} and dominated by a single amino acid residue (SI Table 6). The largest blue shift of a site energy is mainly caused by the positively charged Arg M24, which contributes +260 cm^{-1} to the overall site energy shift of +300 cm^{-1} of Chl 94. Arg M24 is located in the positive region of the difference potential $\Delta\phi_{94}$ of Chl 94, thus leading to a blue shift of the site energy (Figure 8). In the case of Chl 12, the main part of the −170 cm^{-1} site energy shift is caused by the amide dipole of the side chain of Gln A115, which points with its positive end toward the negative part of $\Delta\phi_{12}$, shifting the site energy by −100 cm^{-1} (Figure 8).

In the presumed standard protonation state, the largest red-shift (−700 cm^{-1}) of a site energy (Chl 51) is caused by the negatively charged Asp B113, contributing −500 cm^{-1}. Below, we show, however, that this particular Asp is likely to be protonated (uncharged), which reduces the red-shift significantly. Therefore, Chl 67 becomes the site with the lowest excitation energy. The main contributors are the negatively charged Glu B171 and Glu B327, the positively charged Arg B173, and the polar Tyr B329, Trp B339 and His B340, which contribute between −80 cm^{-1} (His B340) and −160 cm^{-1} (Trp B339) to the overall site energy shift $\Delta E_{67} = -540$ cm^{-1}.

Site energy shifts ΔE_m^{Chl} caused by the charge distribution of other Chls *n* (in their electronic ground state) are in most cases smaller than the shifts caused by the protein, a notable exception being Chl 2, that is, the special pair Chl P_B (Figure 5). For seven Chls, the $|\Delta E_m^{Chl}|$ is larger than 100 cm^{-1} and is mainly caused by three other Chls in the respective environments (SI Table 7).

The influence of the hydrogen bonds on those pigments that have site energy shifts $|\Delta E_m| \geq 140$ cm^{-1} and additionally for Chl 1, that is, the special pair Chl P_A, has been investigated in detail. Hydrogen bonds always lead to a red-shift of the site energy, where the amount of the red-shift depends on the H-bond donor and acceptor (SI Table 8). If the acceptor is the 13^1-keto

group of Chl*a*, the average red-shift is 30 cm^{-1} with a maximum shift of 47 cm^{-1} obtained for Chl 1. Much smaller red-shifts result for the 13^3-methyl ester hydrogen bond acceptor group of Chl*a*. The result that hydrogen bonds always lead to red-shifts can be understood on the basis of the difference potential in Figure 8. It is negative around the 13^1-keto group and around the 13^3-methyl ester group. A hydrogen bond donor from the protein will place a partially positively charged hydrogen atom into the negative difference potential, causing thereby a red-shift of the transition energy. If the methyl-ester group is the acceptor, the red-shifts are much smaller, since the difference potential is smaller for this group. The red-shift caused by H-bonds to the special pair pigment P_A (Chl 1) has been investigated experimentally by site-directed mutagenesis of the donor residues.[5] These experiments revealed that the hydrogen bond network, including the residues Thr A742, Tyr A603, Ser A607 and HOH 19, yields a red-shift of around 100 cm^{-1}.[5] Our calculation yields about half of this value. Please note that in the case of the special pair short-range effects have a large influence on the site energies.[6] These effects could be also influenced by the presence or absence of a hydrogen bond, giving rise to additional shifts not included in the present analysis.

There are two phospholipids (LHG-5003, LHG-5004) that strongly shift (>100 cm^{-1}) the site energies of five Chls (27, 28, 65, 66, 96) due to the negative charge mainly located on the phosphate group (SI Table 9). For Chls 27, 28, 65, 66 the shift caused by the lipids is overcompensated by protein induced shifts, for Chl 96 it is partly compensated. Carotenoids as well as iron sulfur clusters and phylloquinones do not lead to significant site energy shifts in PSI (SI Table 5).

Influence of Nonstandard Protonation Pattern. Out of 78 titratable residues in PSI, 23 are found in a nonstandard protonation state at pH 6.5 and 300 K (SI Tables 10 and 11). In Figure 9, we compare the spectra calculated for a nonstandard protonation state at pH 4, 6.5, and 9 with the spectrum obtained for the standard protonation state and with experimental data. The pH-dependence of the former spectra is rather weak and they are very similar to those obtained for the standard protonation state. A notable change in a spectrum with pH is only found in the high-energy wing of the LD spectrum. However, the changes are smaller than the deviations between calculated and measured (at pH 6.5) spectra and therefore the accuracy of our present calculations is insufficient for predicting any change of the spectrum with pH. The site energies obtained for the nonstandard protonation pattern at pH 6.5 correlate well with those of the standard protonation state (Figure 10, SI Table 4) except for that of Chl 51, which is red-shifted by 500 cm^{-1} in the standard protonation state. This shift is caused by Asp B113, which is calculated to be neutral, that is, in a nonstandard protonation state.

Site Energies of PSI Trimers. PSI is arranged as a homo trimer *in vivo*. In the light of the present finding of the importance of long-range electrostatic interactions, it could be that the intermonomer couplings have an influence on the site energies. Therefore, we performed site energy calculations on whole PSI trimers, including an average over the protonation probabilities of titratable amino acid residues. The high correlation between the monomer and the trimer results (Figure 11) shows that the intermonomer electrostatic interactions have only a minor influence on the site energies of the pigments. The site energies of the pigments in the center of the trimer are influenced stronger by intermonomer couplings than those of the pigments located at the periphery, because of the smaller intermonomer distances in the center (SI Figure S23).

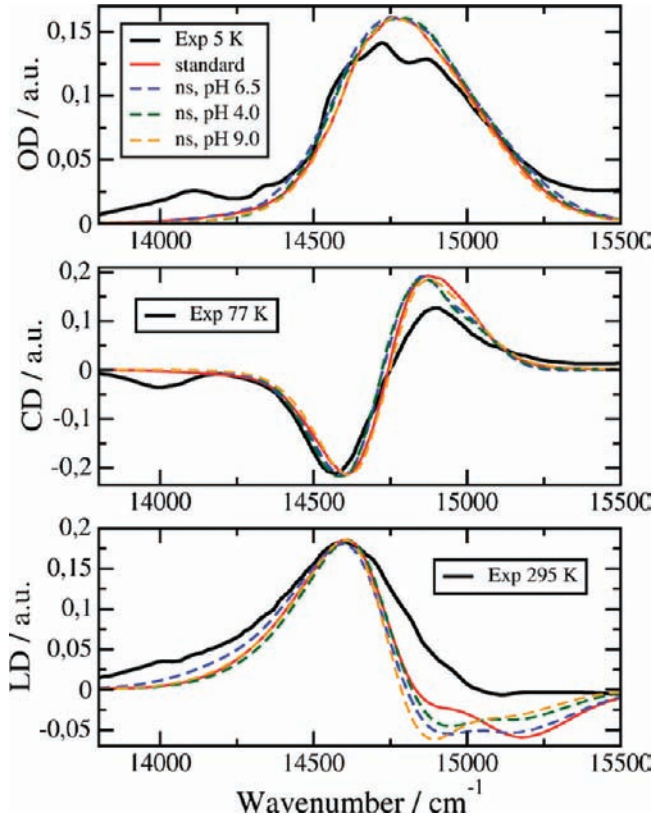

Figure 9. Absorbance at 5 K (top), CD at 77 K (middle), and LD spectra at 295 K (bottom) calculated with site energies obtained from the CDC method using the B65LYP-charge set and pH-dependent partial charges for the protein in nonstandard (ns) protonation state (dashed lines) compared to experimental data[23] (black solid lines) and spectra obtained for standard protonation state (red solid lines, same as in left part of Figure 4).

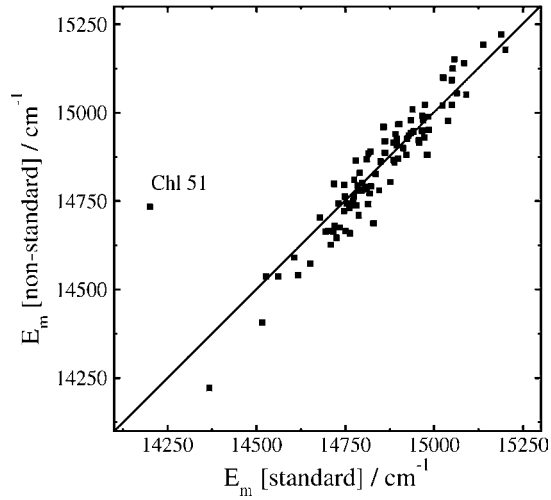

Figure 10. Correlation plot of the site energies resulting for standard and nonstandard protonation states. The numerical values are given in SI Table 4.

Discussion

Excitonic Couplings. Critical points in the structure-based calculation of excitonic couplings are (i) the validity of the simple PD or ED approximations, (ii) the dipole strength of

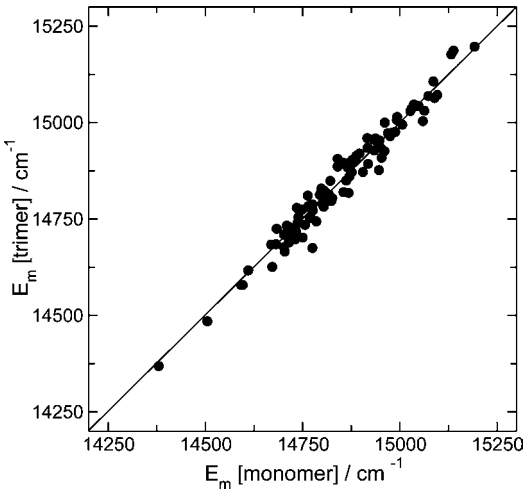

Figure 11. Comparison between site energies calculated for the PSI monomer with those obtained for the whole trimer, taking into account a nonstandard protonation pattern.

the pigments, and (iii) the effect of the dielectric protein environment. In contrast to the BChls in the FMO protein, we find that a PD or ED approximation is not valid for the Chls in PSI (Figure 3). Most likely, the closer packing of pigments in PSI is responsible for this result. Interestingly, in calculations of the excitonic couplings in the special pair of different RCs,[34] we found that an ED approximation with an extent of about 8.7 Å reproduces the transition monopole TrEsp result. The same extent was inferred from studies of the dispersive interaction of BChl and bacteriopheophytin with different nonpolar solvents.[56] Using this extent in the present calculations leads to a large improvement compared to the PD approximation, but there are still significant deviations compared to TrEsp. This result seems to indicate that the optimal dipole extent of the pigments in PSI depends on their mutual orientation.

Concerning the dipole strength of Chl*a* that should be used in the coupling calculations, our results suggest that one can use the vacuum dipole strength $|\mu_{vac}|^2 = 21$ D^2 [37] and explicitly take into account the influence of the dielectric protein environment by the Poisson-TrEsp method. However, practically the same couplings are obtained by using an effective dipole strength $|\mu_{eff}|^2 = f|\mu_{vac}|^2 = 15.1$ D^2 in TrEsp calculations, where the transition monopole charges were rescaled accordingly. This result is interesting in several respects. It shows that for the Chls in PSI the orientation and distance dependence of the factor $f = 0.72$ is weak. A weak dependence was found also for the pigments in the FMO protein, where a somewhat larger value $f = 0.8$ was inferred.[17,18] In contrast, quantum chemical studies that included a dielectric continuum directly in the solution of the Schrödinger equation found a strong distance and orientation dependence of the factor f for a large number of different systems.[43] It remains to be investigated whether those calculations suffer from electron leakage problems, which are avoided in the present two-step approach. The $f = 0.72$ inferred in the present study exactly equals the factor $9\varepsilon_{opt}/(2\varepsilon_{opt} + 1)^2$ that is obtained analytically, if the transition density is approximated by a PD and the molecular cavity by a sphere. Since the PD approximation is not valid for the present system (Figure 3) the agreement of f values can only be caused by an error compensation resulting from the assumption of a spherical cavity. We found a similar error compensation in a study of dispersive lineshifts.[56]

Finally, we note that the excitonic coupling in the special pair (Chls 1 and 2) is dominated by short-range effects,[6] which were neglected in the present analysis. However, this neglect has practically no influence on the spectra presented here due to the large number of antenna pigments (SI Figure S25). As mentioned above, a few antenna pigments give rise to the low energy absorbance peak in the experimental spectrum. For these pigments we expect short-range contributions to the excitonic couplings as well that will be investigated in the near future.

Site Energies and Functional Implications. The present CDC method allows to obtain site energies that describe the optical spectra of PSI core complexes semiquantitatively (Figure 4, SI Figure S18). In particular, the LD spectrum shows that a combined quantum chemical/electrostatic approach yields more reliable site energies than the purely quantum chemical approaches applied so far to PSI (Figure 4). In the approach by Damjanovic et al.,[25] a cutoff radius of 2.5 Å was used and all amino acids with an atom within this distance from any Chl atom were included in the quantum chemical calculations. The present calculations show that the site energies of more than half of the Chls are influenced by more than 20 amino acid residues (Figure 6) and hence long-range electrostatic interactions are indeed important.

In the second quantum chemical treatment,[26] these long-range interactions were included by fixed atomic partial charges. One possible reason for larger errors of the site energies in this case could be the electron leakage effect, that leads to a distortion of the electron density of the pigments. For example, a positive external charge can trap electrons, dependent on the basis set used in the quantum chemical calculations, whereas in reality, the Pauli repulsion between electrons would prevent this leakage.[30] In the present calculations, the leakage problem was avoided by using a two-step procedure, performing the quantum chemical calculations in vacuum first and using the partial charges derived from these calculations afterward in electrostatic calculations. As expected from the difference of optical spectra calculated (Figure 4), the previously calculated structure-based site energies[25,26] do not correlate with the present site energies (correlation plots are given in SI Figure S24).

The large number of pigments makes a determination of site energies by a fit of optical spectra ambiguous. There is no correlation between the present site energies and the values that Byrdin et al.[23] or Brüggemann et al.[24] fitted (SI Figure S24). Nevertheless, the fitted site energies describe the experimental LD spectra better than the present calculations. However, an important advantage of a direct calculation is the possibility to relate spectral shifts to structural elements.

The main results of our analysis of structure - site energy relations are: (i) The major source of site energy shifts is the protein predominantly leading to red-shifts, whereas the Chls, water molecules, and carotenoids have a much smaller influence on site energy shifts. Lipids are found to cause mainly blue-shifts in site energies, which are however, overcompensated by larger red-shifts due to the protein. (ii) The majority of site energies is influenced by a large number of amino acid residues. (iii) The largest blue-shift (Chl 94) is caused by a single amino acid residue and the largest red-shift (Chl 67) of a site energy is caused by interactions with six amino acid residues. Chl 94 is situated at the periphery, whereas Chl 67 is part of a large exciton domain close to the A-branch of the RC (see below).

(56) Renger, T.; Grundkötter, B.; Madjet, M. E.; Müh, F. *Proc. Natl. Acad. Sci. U.S.A.* **2008**, *105*, 13235.

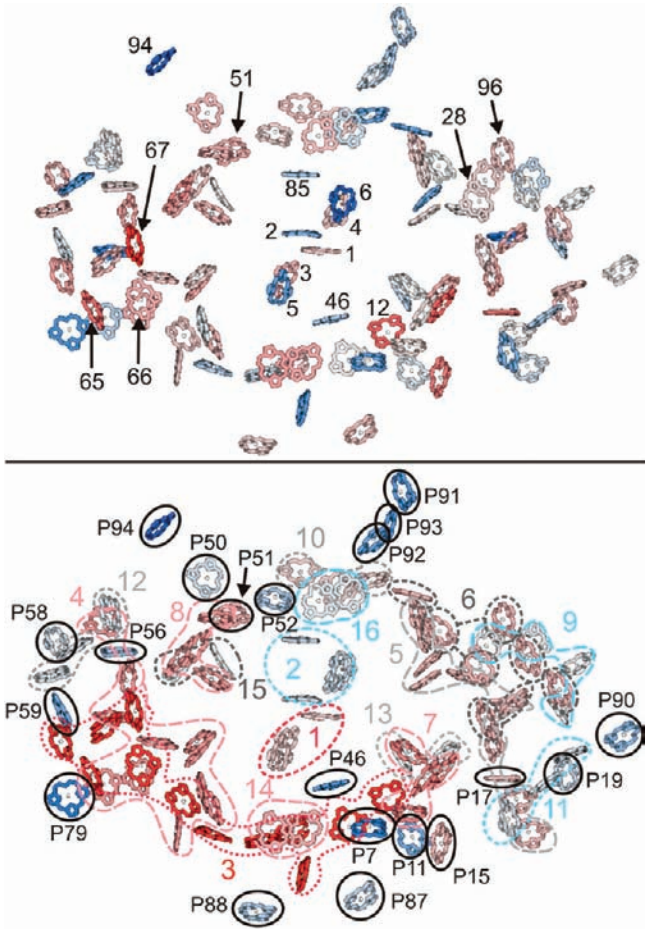

Figure 12. Transition energies depicted in color-code. The stronger the red-shift, the more saturated is the red color, the stronger the blue-shift, the more saturated is the blue color. Numerical values of the lowest exciton energies of the domains and the site energies are given in SI Tables 3 and 4. (Top) Site energies of the 96 Chls. Some Chls are high-lighted by their numbers. (Bottom) Pigments are colored according to the energy of the lowest exciton state of the domain they belong to. For better clarity, the multipigment domains are encircled with dashed colored lines and the domain number is given in the same color. The single-pigment domains are marked with black ellipses and by numbers of the pigments with prefix "P".

(iv) The α-helix dipole moments are not as important as in the FMO protein, where they determine the energy sink.[18,22] This result is due to cancellation effects caused by the antiparallel orientations of nearby helices in PSI. (v) Except for one Chl (Chl 51), the site energies can be well described by assuming a standard protonation pattern of the protein. One might get the impression that one incorrect site energy is not so crucial since the spectrum has contributions from 96 Chls. However, Chl 51 would be incorrectly identified as an excitation energy sink in the core antenna, if a standard protonation state is assumed. Therefore, an evaluation of protonation probabilities is necessary, in particular, if one wants to calculate excitation energy transfer.

An illustration of the site energy values, taking into account the nonstandard protonation pattern, is presented in Figure 12. In the upper part of this Figure, a linear scale between blue and red was used to color the macrocycle of the Chls according to their site energy. In the lower part of this Figure, we have colored all the pigments of one domain in the same way according to the energy of the lowest exciton state of this domain, taking into account an average over disorder in site

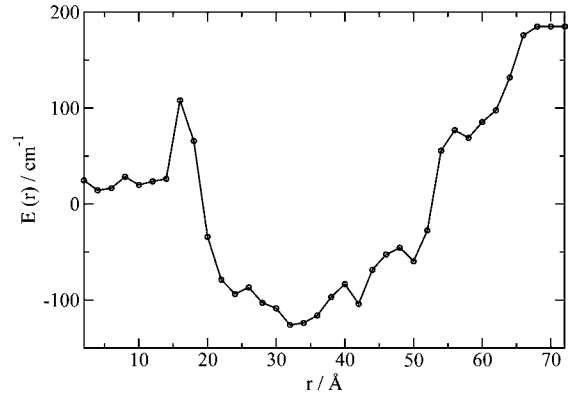

Figure 13. Mean lowest exciton energy $E(r) = 1/N_r\sum_{d=1}^{N_r}\varepsilon_{1d}(r)$ as a function of the radial distance r from the special pair. The lowest exciton energy ε_{1d} of domain d is included in the average, if at least one Chl m in this domain has an atom within a distance r and $r + \Delta r$ from the special pair. N_r is the number of domains that contribute for a given value of r, $\Delta r = 2$ Å was used in the calculations.

energies. To include a possible localization of exciton states by a difference $\Delta E_{mn} = E_m - E_n$ in site energies between pigments m and n, which is not taken into account in the original definition of exciton domains, but is present in the calculation of the spectra, we included a pigment m into a domain, if it is coupled by $V_{mn} > \Delta E_{mn}/6$ to at least one other pigment n of that domain. This criterion is used in addition to the original criterion ($V_{mn} > V_c$). In other words, the new domains shown in Figure 12 (lower part) account for exciton localization due to site energy differences. As can be seen, there is a high concentration of low-energy exciton states on that part of the antenna that is connected to the A-branch of the RC (lower part of the complex in Figure 12). We note also that, since the monomer−monomer interfaces in the PSI trimer are formed by the B-branch side of the monomers, the concentration of low-energy exciton states is found to be higher at the periphery of the trimer.

In Figure 13, the average excitation energy of the antenna is plotted as a function of the radial distance from the special pair, where the energies of the lowest exciton state of the domains are used in the calculation of the average, performing also an average over disorder in site energies. Interestingly, the RC pigments do not form an excitation energy sink. The lowest exciton energies are found at a distance between 25 and 35 Å from the special pair. An excitation energy funnel is visible that guides the excitation energy from the periphery of the antenna to the low-energy exciton states. Recent quantum chemical calculations suggest that the short-range effects between the two special pair Chls in the RC create an excitation energy sink at the special pair.[6] The site energies obtained for the *accessory* Chls Acc_A (Chl 3) and Acc_B (Chl 4) (SI Table 4) are higher by about 500 cm^{-1} than the lowest exciton state of the RC, which is known from mutagenesis studies[5] to absorb at 700 nm and to have a large contribution from the special pair Chl P_A (Chl 1). Taking into account this energy difference, the fact that short-range site energy shifts are only found in the special pair,[6] and that the site energies of the remaining two RC Chls, the primary electron acceptors A_{0A} (Chl 5) and A_{0B} (Chl 6), are higher by 300−400 cm^{-1} than those of Acc_A and Acc_B (SI Table 4), it can be concluded that the lowest exciton state of the RC, in essence, represents the low-energy exciton state of the special pair P_A (Chl 1) and P_B (Chl 2). A detailed analysis of electron exchange effects in the special pair shows that the latter can be included in the present exciton Hamiltonian by shifting the site energies of P_A and P_B by 425 and 500 cm^{-1}

to the red, respectively, and by increasing their excitonic coupling by 185 cm^{-1}.[6] This change of the exciton Hamiltonian will of course have an influence on the trapping of excitation energy by the RC. Its influence on the stationary optical spectra is, however, minor (SI Figure S25), since only two transition energies are affected.

The barrier between the low-energy exciton states of the antenna and the special pair is in the order of the thermal energy at room temperature (Figure 13). Hence, both, thermally activated population of the excited states of the RC and the bridging Chls and trapping by the special pair or direct superexchange-type tunneling to the special pair, or a combination of both are possible mechanisms. In other words, a common theme for all known photosystems could be the relatively slow transfer of the excitation energy to the trap. In the case of the RC of purple bacteria and the RC of photosystem II, the large spatial distance between the RC and the antenna pigments is responsible for this phenomenon. In the case of PSI, it is the energetic barrier created by the high-energy excited states of the RC Chls 3−6 (Acc_A, Acc_B, A_{0A}, A_{0B}) and the bridging Chls 46 (A40) and 85 (B39) between the low-energy exciton states of the antenna and the special pair.

Recent mutagenesis studies suggest that the accessory Chls Acc_A and Acc_B act as primary electron donors in PSI.[3,4] Based on the above arguments, primary ET from the excited Acc_A and Acc_B has to compete with exciton relaxation to the special pair. It is known from the purple bacterial reaction center that selective excitation of the accessory bacteriochlorophyll of the ET active branch can indeed trigger fast ET from there.[57,58] This side pathway is, however, not active in purple bacteria, since the excitation energy of the core light-harvesting complex LH1 is much lower than the energy of excited states of the accessory bacteriochlorophylls and, therefore, the excitation energy is transferred directly from the LH1 to the special pair, from where ET starts. In the case of PSI, the energy difference between the low-energy exciton states of the antenna and the accessory chlorophylls is much smaller (Figure 13) and thermal energy at room temperature is sufficient for excitation energy transfer to Acc_A and Acc_B, from where ET could start.

One explanation for the asymmetric ET along the two branches,[7−13] therefore, is that this asymmetry reflects the asymmetric delivery of excitation energy to Acc_A and Acc_B, due to the larger concentration of low energy exciton states of the antenna near the A-branch of the RC (Figure 12). Since exciton transfer from the accessory Chls to the special pair can be assumed to be ultrafast as well, we expect that a significant part of ET will start from the special pair. If indeed both the accessory and the special pair pigments can act as primary electron donors, the relative weight of the respective processes should be a function of temperature. At low temperature, thermal energy will not be sufficient for excitation energy transfer from the low-energy exciton states of the antenna to the accessory Chls. Hence, the excitation energy will be transferred only to the special pair via superexchange-type tunneling, and ET starts mainly from there. There might still be a fraction of RCs, where ET starts from the accessory Chls due to the small contribution of the latter in the lowest exciton state of the RC, which may be different in different complexes due to disorder in site energies of the RC pigments. However, this fraction should be significantly smaller at low temperature. This effect should give rise to a temperature dependent branching ratio of ET, since only the ET starting at the accessory Chls takes notice of the asymmetry in light-harvesting. Studies of the temperature dependence of primary ET in connection with studies on mutants would be helpful in this respect.

We note that also in the antenna, a few red-absorbing states[28] are most likely created by short-range effects that are beyond the scope of the present analysis. These states give rise to the experimental absorbance peak in the low energy region (Figure 4) that is not reproduced by the present calculations. Hence, we expect a few additional low energy antenna states. From a functional point of view, it could be an advantage to locate these states in the region of the other low energy exciton states, that is, at 25−35 Å distance from the special pair. In this case, it might be possible to tunnel through the barrier formed by the exciton states of the linker pigments 46 and 85 and the RC pigments 3−6 directly to the special pair, from where ET could start. Alternatively, thermal energy under physiological conditions is sufficient for the excitation energy to escape those additional red states to reach the low-energy exciton states depicted in Figure 13.

Conclusion

A structure-based calculation of site energies and excitonic couplings was used to simulate optical spectra of PSI using a minimal number of free parameters: (i) the inhomogeneous width $\Delta_{inh} = 300$ cm^{-1} of the site energy distribution function, (ii) the vacuum transition energy $E_0 = 14\,900$ cm^{-1}, (iii) the effective dielectric constant $\varepsilon_{eff} = 1.5$, and (iv) the Huang−Rhys factor $S = 0.6$ of the exciton-vibrational coupling. The calculated spectra match the experimental data semiquantitatively and allow for a detailed analysis of structure−function relationships. Three important results of this analysis are: (i) The site energies of most Chls are determined by interactions with a large number of amino acid residues indicating the importance of long-range electrostatic interactions. (ii) The special pair appears to be isolated from the low-energy exciton states of the antenna by intermediate high-energy exciton states. (iii) The concentration of low-energy exciton states is higher on the side of the antenna that is connected to the A-branch of the reaction center.

For the resulting asymmetry in light-harvesting to affect the branching ratio of ET, the latter would have to start at the accessory Chls. Indeed, it was inferred from experiments on mutants that these Chls act as primary electron donors.[3,4] However, the energetics of excited states in the RC, as revealed from studies on mutants,[5] quantum chemical calculations[6] and the present site energy values, suggests that the excitation energy sink is located at the special pair. A possibility might be the presence of two ET pathways per branch, one starting at the special pair and one at the accessory Chls. Only the latter is sensitive to the asymmetric delivery of excitation energy from the antenna and thus occurs more rapidly along the A-branch. The relative weight of the former increases at low temperatures, when the excitation energy is transferred via superexchange type tunneling directly from the low-energy antenna states to the special pair without intermediate population of the excited states of the accessory Chls. If this hypothesis is true, the branching ratio should be temperature dependent, an effect that can be investigated experimentally.

Acknowledgment. We thank N. Krauss for providing corrected coordinates for Chl*a*′. Support by the Deutsche Forschungsgemein-

(57) van Brederode, M. E.; Jones, M. R.; van Mourik, F.; van Stokkum, I. H. M.; van Grondelle, R. *Biochemistry* **1997**, *36*, 6855.
(58) van Brederode, M. E.; van Mourik, F.; van Stokkum, I. H. M.; Jones, M. R.; van Grondelle, R. *Proc. Natl. Acad. Sci. U.S.A.* **1999**, *96*, 2054.

schaft through Sonderforschungsbereich 498 (TP A7) and Cluster of Excellence UniCat is gratefully acknowledged. We thank Gernot Kieseritzky and Prof. E. W. Knapp for advice in performing the electrostatic calculations.

Supporting Information Available: Complete refs 40 and 45, atomic partial charges obtained for the ground and excited states of Chl*a* using different quantum chemical methods, excitonic couplings calculated with different methods, characterization of exciton domains in Figure 12, site energies obtained with TDDFT/B65LYP for standard and nonstandard protonation patterns, contributions of different parts of the pigment−protein complex (protein, lipids, explicit water, Chls, carotenoids, phylloquinones) to site energy shifts, site energy shifts due to selected single amino acid residues, selected Chls, hydrogen bonds and lipids, protonation probabilities of titratable amino acid residues in nonstandard state, comparison of spectra calculated with Poisson-TrEsp couplings with those obtained with TrEsp and $f = 0.72$, temperature dependence of absorbance spectra, spectra calculated for different threshold values V_c used in the definition of exciton domains, comparison of optical spectra obtained with atomic partial charges from different quantum chemical methods, comparison between present calculations and results of Yin et al.,[26] site energy shifts resulting from interaction with the backbone of α-helices and with transmembrane α-helices, influence of intermonomer couplings in PSI trimers on site energy shifts, correlation plot between present site energies and those obtained by Yin et al.,[26] Damjanovic et al.,[25] Byrdin et al.[23] and Brüggemann et al.,[24] comparison of optical spectra obtained for different inhomogeneous widths and effective dielectric constants, influence of short-range excitonic effects in the special pair on optical spectra. This material is available free of charge via the Internet at http://pubs.acs.org.

JA9072222